IET Electric Power Applications

Research Article

IET Journals
The Institution of Engineering and Technology

Direct torque and flux control of interior permanent magnet synchronous machine in deep flux-weakening region

ISSN 1751-8660
Received on 4th March 2017
Revised 31st July 2017
Accepted on 17th August 2017
E-First on 20th September 2017
doi: 10.1049/iet-epa.2017.0147
www.ietdl.org

Sithumini Ekanayake[1] ✉, Rukmi Dutta[1], M. Faz Rahman[1], Dan Xiao[1]

[1]*School of Electrical Engineering and Telecommunications, University of New South Wales, Sydney, Australia*

✉ *E-mail: p.ekanayake@unsw.edu.au*

Abstract: Direct torque and flux control (DTFC) is known for its reduced torque and flux ripples compared to the classical direct torque control scheme. It can drive an interior permanent magnet synchronous motor (IPMSM) in usual control regimes while satisfying current and voltage limits of the system. However, deep flux-weakening control of an IPMSM under DTFC has not been investigated as extensively, especially operation along the maximum torque per voltage (MTPV) trajectory in the torque-flux plane. This study proposes a simple and effective control method, which incorporates MTPV trajectory in the conventional flux-weakening algorithm of DTFC. Performance of an IPMSM drive is analysed when operated with the proposed control method.

1 Introduction

Among various control techniques, the direct torque control schemes are proven to provide simplicity, fast dynamic response and less parameter dependency compared to the current vector control schemes [1–4]. The classical direct torque control (DTC) scheme which uses hysteresis controllers and a switching table is widely used in driving electrical motors position sensorlessly, because the estimation of torque and flux can be carried out in the stationary reference frame [5]. However, one of the main drawbacks of classical DTC is the unavoidable large ripple in the torque and flux responses. As an alternative, a modified DTC scheme which reduces torque and flux ripples was proposed in [6–8] for an interior permanent magnet synchronous machine (IPMSM) drive. The proposed method replaces hysteresis controllers and the switching table of classical DTC with a PI controller and space vector modulation. Even though this method is known to provide reduced flux and torque ripples, it is comparatively noisy and complex [7]. The modified DTC later evolved as direct torque and flux control (DTFC) scheme and gained the attention of the research community as it can provide far less torque and flux ripples while retaining the desirable features of classical DTC [9]. In the DTFC scheme, two PI controllers are used in order to regulate the torque and flux individually.

Many high-performance industrial drives prefer interior permanent magnet synchronous motors due to their desirable characteristics such as high efficiency, flux-weakening capability and compact size. The flux-weakening capability is indeed an advantage to an IPMSM, because it allows the motor to achieve a wide speed range under the system constraints. Ability to operate in a wide speed range brings the benefit of efficient energy utilisation. Typically, trajectory control is implemented in IPMSM drives to achieve optimum torque performance at the constant torque and power regions [10–12]. Current vector controlled IPMSM drives use maximum torque per ampere (MTPA) trajectory, current and voltage limit trajectory and maximum torque per voltage (MTPV) trajectory defined on i_d–i_q plane for the efficient operation of the motor over a wide speed range. It is noteworthy that the MTPV trajectory control can be applied only if the characteristic current (ratio of magnet flux-linkage over the d-axis inductance) of the IPMSM is less than the rated current. If the characteristic current happens to be larger than the rated current, MTPV trajectory lies outside to the current limit circle in the i_d–i_q plane as shown in Fig. 1*a* and cannot be incorporated in the control algorithm. The MTPV trajectory which is also known as voltage limited maximum output trajectory and maximum torque per flux (MTPF) trajectory was used to extend the motor speed to the deep flux-weakening region by minimising flux for maximum torque [11, 13–17] when the machine rated current is larger than the characteristic current. The trajectories defined on i_d–i_q plane for current controlled IPMSM drives can be incorporated in the DTC schemes by transforming them to torque (T)–flux (λ) plane [18, 19]. It was shown in [19] that operating along the MTPA, current and voltage limit trajectories defined on T–λ plane can deliver satisfactory results for low and medium speed operations of IPMSM drives under DTFC scheme. However, operation in the deep flux-weakening region along the MTPV trajectory defined on T–λ plane was not discussed in these papers.

Various implementation methods of MTPV control under classical DTC scheme were discussed in [20–22]. The method proposed in [20] uses an analytical equation to generate the flux reference for trajectory control in IPMSM. The analytical and numerical techniques presented in this paper were complex and no flux-weakening speed range was included in the results. The method presented in [21] uses MTPV control to achieve optimal efficiency operation. However, the method heavily relies on the look-up tables, which need to be pre-determined from experiments or FEA calculations, and may not be easy to implement directly on an industrial drive. The control scheme of [22] modifies the flux reference and torque limit according to the torque error and extends the flux-weakening operation up to the MTPV control region. However, the proposed method of [22] was presented through simulation study only, no experimental verification was provided. In [23], a method based on the maximum torque angle was proposed for the modified DTC scheme, but the MTPV trajectory in the T–λ plane was not shown.

In this paper, a new method to include MTPV control in DTFC is proposed and the effectiveness of the proposed method has been verified by the experimental implementation. It was shown that by operating the machine along the optimum control trajectories defined on T–λ plane, the load angle can be maintained below the maximum allowed load angle. Specially, when MTPV trajectory control is carried out, it ensures maximum load angle under minimum flux condition and the load angle is maintained at or slightly below the limit at all times. A preliminary study of a direct toque and flux controlled IPMSM in the deep flux-weakening region using MTPV trajectory control was reported in [24]. This paper extends the work presented in [24] by further analysing the results obtained from experimental implementation. The experimental results were obtained by operating the drive system

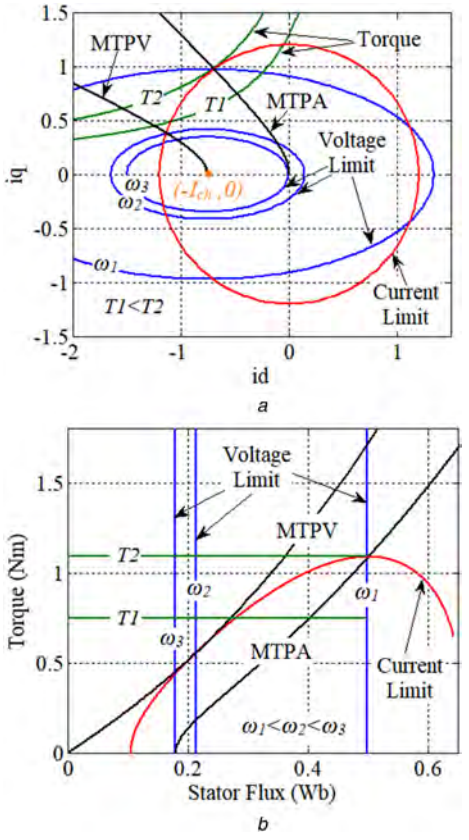

Fig. 1 *Trajectories in*
(a) i_d–i_q plane, ***(b)*** T–λ plane

position sensorlessly over a wide speed range. If parameter variation is not significant in a machine, implementation of the proposed method is simple because it only depends on the optimum control trajectories of the IPMSM derived off-line using machine dq model and does not require any prior experimental work except finding motor dq parameters. If parameter variation is significant in a machine, the proposed method can also be modified by incorporating online parameter estimation techniques available in the literature [25–27].

This paper is organised as follows. After this introduction, a brief description about the DTFC scheme is presented in Section 2. Then the proposed control method is explained in Section 3. In Section 4, experimental results are presented for the proposed position sensorless drive implemented on an IPMSM. Section 5 concludes the paper.

2 Direct torque and flux control

2.1 Principle of DTFC in an IPMSM

The mathematical model of an IPMSM in the rotor reference frame is given below:

$$v_d = R_s i_d + L_d \frac{\mathrm{d}i_d}{\mathrm{d}t} - \omega_r L_q i_q \tag{1}$$

$$v_q = R_s i_q + L_q \frac{\mathrm{d}i_q}{\mathrm{d}t} + \omega_r L_d i_d + \omega_r \lambda_f \tag{2}$$

v_d, v_q, i_d, i_q, L_d and L_q are d-axis and q-axis voltages, currents and inductances, respectively. R_s, λ_f and ω_r are stator resistance, permanent magnet flux linkage and electrical angular velocity of the rotor, respectively.

By using reference frame transformations, it can be shown that the electromagnetic torque (T) of the machine in the stator reference frame is [5]

$$T = \frac{3}{2} p |\lambda_s| i_y \tag{3}$$

where λ_s and p are the stator flux linkage and number of pole pairs of the machine. Equation (3) shows that the torque is directly proportional to the y-axis component of the stator current, if the amplitude of the stator flux linkage λ_s is a constant.

Equations (1) and (2) can be represented in the stator reference frame as (4) and (5), where ω_s is the speed of the stator flux vector [9]

$$v_x = R_s i_x + \frac{\mathrm{d}\lambda_x}{\mathrm{d}t} = R_s i_x + \frac{\mathrm{d}|\lambda_s|}{\mathrm{d}t} \tag{4}$$

$$v_y = R_s i_y + \omega_s \lambda_x = \frac{2R_s}{3p|\lambda_s|} T + \omega_s \lambda_s \tag{5}$$

Equations (4) and (5) show that the stator flux and torque can be regulated by the x- and y-axis components of the stator voltage. Based on this, two PI controllers are used in the DTFC scheme to regulate the stator flux and torque. The output of the PI controllers generates x- and y-axis components of the stator voltage which can be transformed to $\alpha\beta$ stationary reference frame to generate the space vector modulation for the inverter.

The stator flux linkage and electromagnetic torque in the $\alpha\beta$ stationary reference frame can be estimated using (6). The estimated torque and stator flux linkage are used as the feedback to the PI controllers for the closed-loop torque and flux control

$$\begin{aligned} |\lambda_s| &= \sqrt{\lambda_\alpha^2 + \lambda_\beta^2} \\ T &= \frac{3}{2} p(\lambda_\alpha i_\beta - \lambda_\beta i_\alpha) \end{aligned} \tag{6}$$

where $\lambda_\alpha = \int (V_\alpha - R_s i_\alpha)\,\mathrm{d}t$ and $\lambda_\beta = \int (V_\beta - R_s i_\beta)\,\mathrm{d}t$.

2.2 Trajectory control for DTFC

The MTPA, MTPV, current and voltage limit trajectories defined on the T–λ plane are incorporated in the DTFC scheme to achieve the optimum operation of IPMSM drive.

2.2.1 MTPA trajectory: The MTPA trajectory defined on the i_d–i_q plane can be transformed to T–λ plane by calculating torque and stator flux for each i_d and i_q pair using as

$$\begin{aligned} T &= \frac{3}{2} p\left[\lambda_f + (L_d - L_q) i_d\right] \sqrt{i_d^2 - \frac{\lambda_f}{(L_q - L_d)} i_d} \\ \lambda_s &= \sqrt{\lambda_f^2 + \left[2L_d - \frac{L_q^2}{(L_q - L_d)}\right] \lambda_f i_d + (L_d^2 + L_q^2) i_d^2} \end{aligned} \tag{7}$$

Figs. 1*a* and *b* show the MTPA trajectory in the i_d–i_q and T–λ plane, respectively.

2.2.2 Current and voltage limit: The constraints of current and voltage in the i_d–i_q plane are given in (8) and (9). I_{sm} and V_{sm} are the maximum available current and voltage. Usually the voltage drop due to the armature resistance is pre-compensated in the voltage limit

$$\sqrt{i_d^2 + i_q^2} \le I_{sm} \tag{8}$$

$$\sqrt{v_d^2 + v_q^2} \le V_{sm} \tag{9}$$

The current limit can be plotted in the T–λ plane by calculating torque and stator flux using (10) for each i_d and i_q pair in (8)

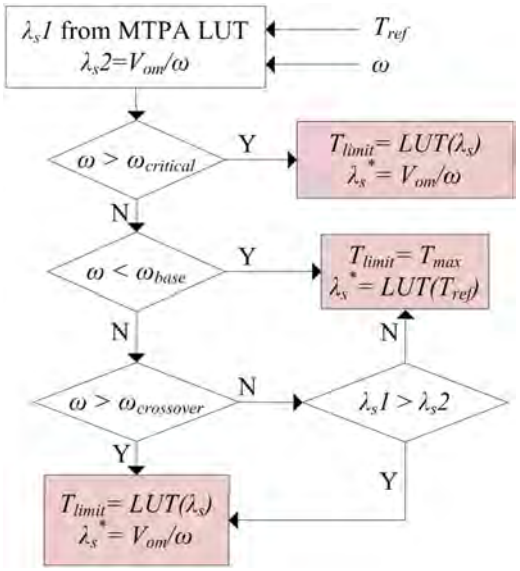

Fig. 2 *Selection of torque and flux reference for each control mode*

$$\lambda_s = \sqrt{(\lambda_f + L_d i_d)^2 + (L_q i_q)^2}$$
$$T = \frac{3}{2} p[\lambda_f i_q + (L_d - L_q) i_d i_q] \tag{10}$$

If the stator resistance drop is neglected, the stator voltage is proportional to the rotor speed ω_r and stator flux linkage λ_s, as shown in (11), which gives the voltage limits in the T–λ plane for various speeds

$$\omega_r |\lambda_s| = V_{sm} \tag{11}$$

The voltage limit trajectories in the i_d–i_q and T–λ plane are, respectively, as shown in Figs. 1*a* and *b* for base speed (ω_1, maximum speed at constant maximum torque is available), critical speed (ω_2, minimum speed for the voltage limited maximum output operation) and crossover speed (ω_3, speed at which the back EMF reaches the limiting value) of an IPMSM. The voltage limit trajectories of various speeds which are concentric ellipses in the i_d–i_q plane become vertical lines in the T–λ plane.

2.2.3 MTPV trajectory: Flux-weakening control allows an IPMSM to achieve a wider speed range under voltage and current constraints of the system. As explained in Section 1, if the characteristic current of the IPMSM is less than the rated current, MTPV trajectory control can be carried out to extend the motor speed further in the flux-weakening region. The relationship between i_d and i_q for MTPV control is given in (12) [11]

$$i_d = -\frac{\lambda_f}{L_d} - \Delta i_d$$
$$i_q = \frac{\sqrt{(V_{sm}/\omega_r)^2 - (L_d \Delta i_d)^2}}{L_q} \tag{12}$$

where

$$\Delta i_d = \frac{-L_q \lambda_f + \sqrt{(L_q \lambda_f)^2 + 8(L_q - L_d)^2 (V_{sm}/\omega_r)^2}}{4 L_d (L_q - L_d)}$$

Torque and flux can be calculated using (10) for each i_d and i_q pair given by (12) to plot the MTPV trajectory in the T–λ plane. The MTPV trajectory in i_d–i_q and T–λ plane are also shown in Figs. 1*a* and *b*, respectively.

3 Proposed control method

3.1 Trajectory control for a wide speed range

Conventionally, MTPA, current and voltage limit trajectories defined on T–λ plane are used in constant torque and flux-weakening operations. However, flux-weakening range of a motor can be significantly increased by carrying out MTPV trajectory control as it provides the maximum torque under minimum flux condition.

For MTPA operation under DTFC, torque reference is determined by limiting the output of the speed controller to the maximum torque that can be gained with MTPA control, which is the intersection of MTPA trajectory and current limit trajectory. The stator flux linkage reference for MTPA control is selected from a look-up table. The look-up table can be constructed by finding the stator flux linkage for each torque value on the MTPA trajectory. For conventional flux-weakening operation, the torque reference is obtained by limiting the output of the speed controller to the intersecting points of current and voltage limit trajectories. To implement this, a look-up table based on the torque values of the intersecting points can be used. The stator flux reference for flux-weakening operation is calculated from (11). The torque reference for MTPV control can be obtained from a look-up table that limits the speed controller output according to the MTPV trajectory. Similar to the conventional flux-weakening control, the stator flux reference for MTPV control is calculated from (11). In the proposed method, look-up tables are not necessary to obtain the torque and flux references for MTPA and flux-weakening control. By using curve fitting techniques, it is possible to derive equations for each trajectory on the T–λ plane which can be directly used in the control scheme. However, by implementing look-up tables, computational time can be greatly reduced.

In the proposed method, control along each trajectory is decided based on the motor speed and load torque. Initially, the motor speed is checked for the MTPV condition. If the motor speed is greater than the critical speed, torque limit and flux reference are selected according to the MTPV trajectory. If the motor speed is below base speed, MTPA trajectory is selected for any load. If the motor speed is above base speed and below crossover speed, MTPA control or flux-weakening control is applied depending on the load. Between base speed and crossover speed, if the applied load is high enough for back EMF to reach its limiting value, flux-weakening control needs to be selected, otherwise MTPA control is carried out. As the stator flux-linkage of the machine is proportional to the developed voltage, switching between MTPA and flux-weakening control in DTFC is decided by comparing stator flux-linkage under MTPA and flux-weakening operations as shown in Fig. 2. If the motor speed is greater than crossover speed, flux-weakening control is needed for any load condition. The summary of selection criteria is shown in Fig. 2.

3.2 Load angle control

The variation of load angle (δ) with the stator flux linkage under trajectory control is shown in Fig. 3. The maximum allowable load angle ($\delta_{\max}$) for the stable operation of IPMSM can be calculated from (13) [18]

$$\delta_{\max} = \cos^{-1}\left[\frac{1}{4}\left(\frac{a}{|\lambda_s|} - \sqrt{\left(\frac{a}{|\lambda_s|}\right)^2 + 8}\right)\right] \tag{13}$$

where $a = \lambda_f L_q/(L_q - L_d)$.

It was found that the calculated load angle for the MTPV trajectory coincides with the $\delta_{\max}$. Consequently, if the IPMSM is controlled along the MTPV trajectory defined on T–λ plane, the load angle never exceeds its limit ($\delta_{\max}$) as depicted in Fig. 3. The torque expression in terms of the amplitude of the stator flux linkage and load angle was given in [18]. If maximum load angle is used in the torque expression as shown in (14), it generates an equivalent torque as MTPV trajectory for a specific stator flux linkage. Therefore, to limit the torque for MTPV control, either a look-up table based on the trajectory or (14) can be used

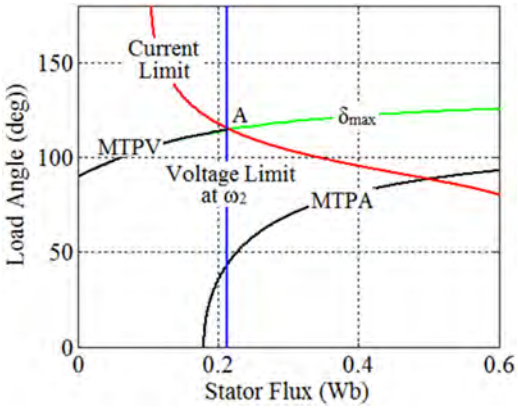

Fig. 3 *Variation of load angle under trajectory control*

$$T_{\text{mtpv}} = \frac{3p|\lambda_s|}{4L_dL_q}\left(2\lambda_f L_q \sin\delta_{\max} - |\lambda_s|(L_q - L_d)\sin 2\delta_{\max}\right) \quad (14)$$

Inoue *et al.* [23] also suggests (14) for the MTPV control of a drive system operated under modified DTC. However, the paper did not discuss the relationship between the MTPV trajectory and the maximum load angle condition. According to Fig. 3, it is clear that the drive system can become unstable, if the motor is operated along the current limit trajectory after 'A', due to the exceeding of the maximum load angle. As explained above, this instability can be eliminated by operating along the MTPV trajectory which automatically allows the maximum load angle operation of the IPMSM. However, realising maximum load angle operation in the experiment can be difficult, as the system tends to become unstable when operated at the limit. Therefore, the torque reference needs to be limited to a value slightly less than the theoretical value given by (14).

3.3 Adaptive sliding mode observer (SMO) for flux estimation

The closed-loop flux estimation techniques such as extended Kalman filter and SMO are typically used in very low speed sensorless drives, because the small back EMF generated at low speed is not sufficient to estimate the rotor position [28, 29]. The problem with the back EMF-based open-loop flux estimation at medium- and high-speed is the voltage integration, which suffers from the dc offset and drift of the feedback signals. To minimise the effect, a first-order low-pass filter can be used instead of the pure integrator [30]. However, selecting a proper filter cut-off frequency such that the flux estimation is carried out accurately over a wide speed range is challenging. Therefore, instead of open-loop flux estimation, SMO-based flux estimation method was selected in this paper to carry out the sensorless operation satisfactorily in the medium- and high-speed range. The adaptive SMO explained in [29, 31] was adopted in this paper. It simultaneously estimates stator flux linkage, speed and rotor position. The structure of the observer is briefly presented below.

The adaptive flux observer can be expressed in the estimated rotor reference frame by considering stator current and flux components as the output and state variables

$$\begin{bmatrix}\dot{\hat{\lambda}}_d\\ \dot{\hat{\lambda}}_q\end{bmatrix} = \begin{bmatrix}-\frac{R_s}{L_d} & \hat{\omega}_r\\ -\hat{\omega}_r & -\frac{R_s}{L_q}\end{bmatrix}\begin{bmatrix}\hat{\lambda}_d\\ \hat{\lambda}_q\end{bmatrix} + \begin{bmatrix}v_d\\ v_q\end{bmatrix} + \begin{bmatrix}\frac{R_s\lambda_f}{L_d}\\ 0\end{bmatrix} + \boldsymbol{KS} + \boldsymbol{\phi}\,\text{sign}(\boldsymbol{S}) \quad (15)$$

$$\begin{bmatrix}\hat{i}_d\\ \hat{i}_q\end{bmatrix} = \begin{bmatrix}\frac{1}{L_d} & 0\\ 0 & \frac{1}{L_q}\end{bmatrix}\begin{bmatrix}\hat{\lambda}_d\\ \hat{\lambda}_q\end{bmatrix} - \begin{bmatrix}\frac{\lambda_f}{L_d}\\ 0\end{bmatrix} \quad (16)$$

The superscript $\wedge$ denotes estimated values and $\boldsymbol{K}$ and $\boldsymbol{\phi}$ are feedback gains of the observer. The sliding hyperplane $\boldsymbol{S}$ is defined on the basis of the stator current errors. The estimation error dynamics of the state variables are as follows. The superscript $\sim$ denotes estimated errors

$$\begin{bmatrix}\dot{\tilde{\lambda}}_d\\ \dot{\tilde{\lambda}}_q\end{bmatrix} = [\boldsymbol{A} - \boldsymbol{KC}]\begin{bmatrix}\tilde{\lambda}_d\\ \tilde{\lambda}_q\end{bmatrix} + \tilde{\omega}_r\begin{bmatrix}\hat{\lambda}_q\\ -\hat{\lambda}_d\end{bmatrix} - \boldsymbol{\phi}\,\text{sign}(\boldsymbol{S}) \quad (17)$$

where

$$\boldsymbol{A} = \begin{bmatrix}-\frac{R_s}{L_d} & \omega_r\\ -\omega_r & -\frac{R_s}{L_q}\end{bmatrix}, \quad \boldsymbol{C} = \begin{bmatrix}\frac{1}{L_d} & 0\\ 0 & \frac{1}{L_q}\end{bmatrix}$$

From the Lyapunov stability theorem, an update law can be derived for the rotor speed estimation [31] and it can be further modified to a PI estimator as shown in (18) for the improved dynamic behaviour of the speed estimation

$$\hat{\omega}_r = (K_{sP} + K_{sI}/S)\cdot\left(\hat{\lambda}_q\tilde{\lambda}_d - \hat{\lambda}_d\tilde{\lambda}_q\right) \quad (18)$$

K_{sP} and K_{sI} are the proportional and integral gains of the PI estimator. The estimated speed is used in the adaptive model of the observer and speed control loop after low-pass filtering. The integral of the estimated speed gives the rotor position. The block diagram of the adaptive observer and DTFC scheme is given in Fig. 4. The estimated flux components obtained from the observer are used to estimate the magnitude of the stator flux linkage and electromagnetic torque as

$$\begin{aligned}\left|\hat{\lambda}_s\right| &= \sqrt{\hat{\lambda}_d^2 + \hat{\lambda}_q^2}\\ \hat{T} &= \frac{3}{2}p\left(\hat{\lambda}_d i_q - \hat{\lambda}_q i_d\right)\end{aligned} \quad (19)$$

4 Results and discussions

This section presents experimental results of the IPMSM operated with the DTFC scheme described in Sections 2 and 3. The experimental setup is shown in Fig. 5*a*. The IPMSM which has parameters as shown in Table 1 was powered through an IGBT inverter equipped with isolated DC supply, voltage and current sensors and protection circuit. The motor was loaded by a direct coupled three-phase servo motor and a torque transducer was used to measure the shaft torque. The control algorithms were implemented on a DS1104 controller board. Experimental inductances of the studied IPMSM shown in Fig. 5*b* demonstrate that the inductance variation is not significant, even for high load conditions. Therefore, constant parameter values were used in the control algorithm throughout the experiment.

A rotary encoder was used to measure the rotor position and speed at the start-up and low speed operation. At medium and higher speeds, the drive system was operated sensorlessly while position and speed from the encoder was used only to verify the estimated speed and rotor position. It should be noted that it is possible to operate the motor sensorlessly at zero and very low speed, using techniques such as high frequency signal injection. However, since this study concerns deep flux-weakening speed range, sensorless operation at very low speed or standstill was not attempted. The controller gains and feedback gains of the SMO were obtained as shown in Table 2, by online tuning of the system.

4.1 Dynamic performance of the IPMSM drive under sensorless DTFC

The experimental results obtained from the direct torque and flux controlled IPMSM drive under a step-load change at base speed is shown in Fig. 6. Initially, the IPMSM was run at the base speed of 1500 rpm under no load condition, and then the full load was applied at $t = 1$ s. At $t = 4.6$ s, the load torque was removed and the machine returns to the no load condition. The response times for

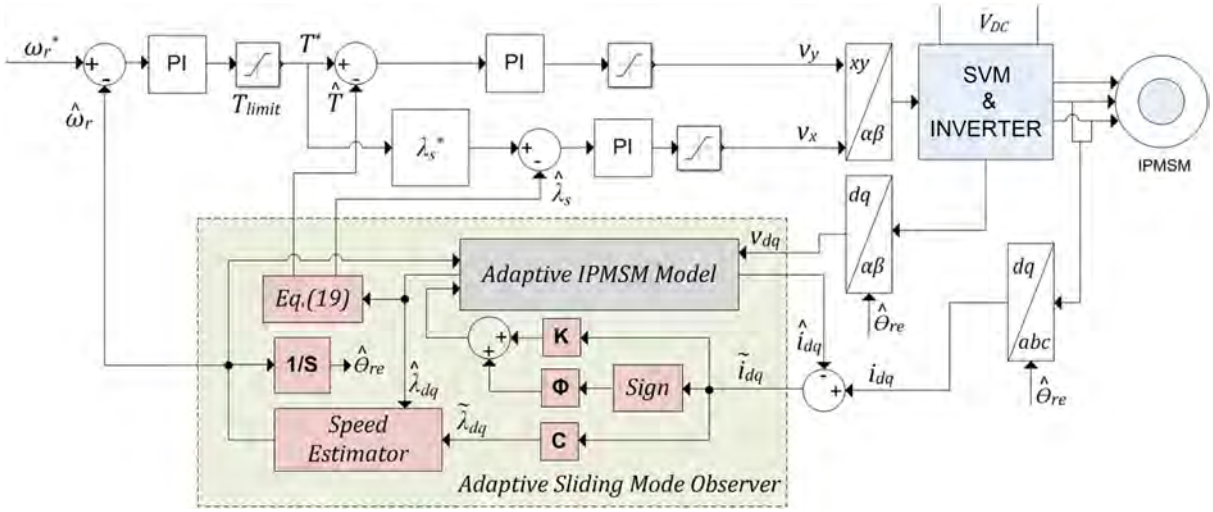

Fig. 4 *Sensorless direct torque and flux control scheme*

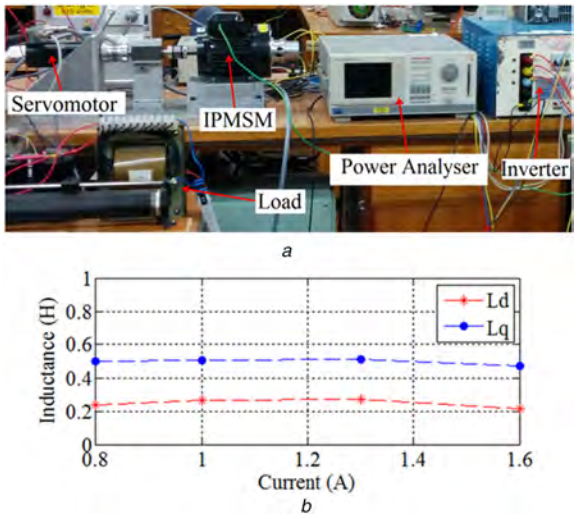

Fig. 5 *Experimental results of the IPMSM*
(a) Experimental setup, ***(b)*** Experimental inductances of the IPMSM

Table 1 Parameters of the IPMSM

Parameter, unit	Value
number of pole pairs	2
stator resistance, Ω	18.6
magnet flux linkage, Wb	0.18
d-axis inductance, H	0.238
q-axis inductance, H	0.5128
rotor inertia, kgm^2	0.00117
rated phase voltage, V	178
rated phase current, A	1.2
base speed, rpm	1500

Table 2 Experimental parameters of the controllers and SMO

Speed controller	Torque controller	Flux controller	SMO	Speed estimator
$K_{pSpd} = 5.8$	$K_{pT} = 600$	$K_{pF} = 800$	$k_1 = k_2 = 600$	$K_p = 500$
$K_{iSpd} = 0.03$	$K_{iT} = 20$	$K_{iF} = 30$	$\phi_1 = \phi_2 = 0.005$	$K_i = 100$

loading and unloading are different, because it depends on the available acceleration torque in the motor during loading and unloading. As shown in Fig. 6, the torque available for the motor to accelerate back to the reference speed during loading is ∼0.1 Nm. In contrast, during unloading, a torque of 0.85 Nm is available for the motor to return to its speed reference. Due to this reason, a fast dynamic response can be expected for unloading. The speed, torque, flux and load angle responses given in Fig. 6 indicate a fairly good dynamic performance of the sensorless IPMSM drive at the base speed. The load angle is maintained at ∼90° for the rated load condition under MTPA control, as theoretically suggested in Fig. 3 (intersection point of MTPA and current limit trajectory).

To observe the dynamic performance with flux-weakening control, acceleration of the IPMSM from 1000 to 4500 rpm under no load was considered. After the critical speed of 3500 rpm, MTPV trajectory control was implemented in the control scheme to obtain the wide speed range. The experimental results are shown in Fig. 7. A smooth transition among MTPA, flux-weakening and MTPV operations was achieved under the proposed method. The steady-state torque and flux ripples at 4500 rpm are ∼3.71 and 3.84% of rated torque and flux. The variation of the load angle and motor current are also shown in Fig. 7. Fig. 7 clearly illustrates the maximum load angle allowed and the load angle of the system which happens to lie below the limit, particularly in the MTPV control region. Theoretically, when the motor is operated under MTPV control, the load angle of the system should equal to the maximum load angle. However, it is difficult to operate the motor in the maximum load angle condition practically, because during transients, it tends to make the system unstable even for a slight exceeding of the allowed maximum load angle. Therefore, a trade-off needs to be made between the stability and maximum torque under MTPV control, if the wide-speed-range operation is intended. This is typically done by reducing the torque limit given by (14) from a factor k where $0 < k < 1$ [23]. However, in this paper, the integral gain of the PI estimator was carefully selected such that the torque and flux control is carried out accurately over a wide speed range while the load angle is maintained below the limit. Fig. 8 shows the operating trajectory on the T–λ and i_d–i_q plane for the acceleration of IPMSM.

4.2 Steady-state performance of the IPMSM drive under sensorless DTFC

The experimental results of the motor at the speed of 4000 rpm with full load under MTPV control are shown in Fig. 9*a*. The estimated speed, torque and flux plotted with their references indicate that the sensorless control of the IPMSM is performed adequately at the full load condition. The stator flux linkage and peak current are at 0.185 Wb and 0.9 A, respectively, for the full load of 0.45 Nm. The torque and flux ripples are within an acceptable limit of ∼9.25 and 12.8% of the rated torque and flux. Note that the load angle of the system is at 95° while the maximum lies at 113°.

Fig. 9*b* shows estimation errors at 4000 rpm under the full load condition. The speed error is bounded within 2 rpm but its average

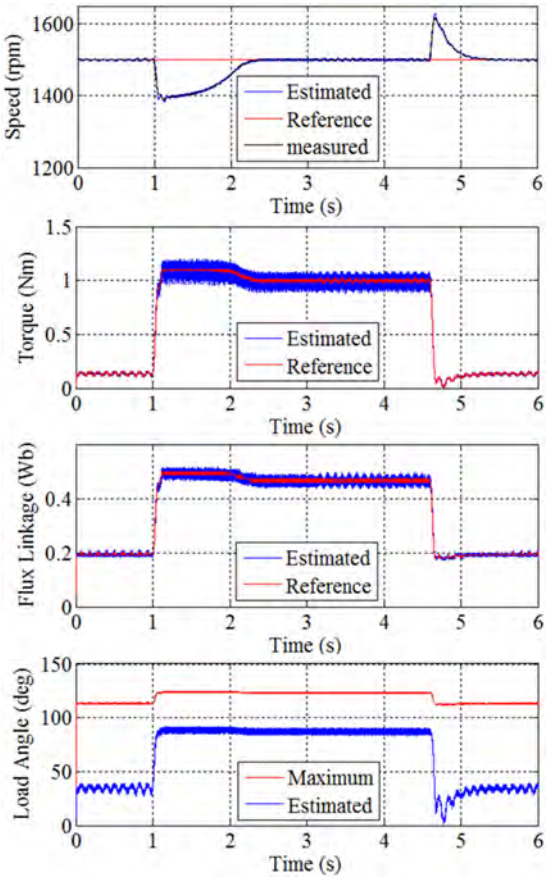

Fig. 6 *Experimental results of the sensorless controlled IPMSM drive under a step load change at 1500 rpm*

is zero. The position error is about 0.22 electrical radians on average. Fig. 9*b* also shows the estimated and calculated $\alpha\beta$ stationary reference frame flux components at 4000 rpm under full load condition. The estimated flux linkage is obtained from the SMO. The measured d–q-axis currents are used in (10) to obtain the calculated flux linkages. Typically, the effect of noise and other disturbances of the motor due to flux-weakening at high speeds, especially with full load, is reflected in the d–q-axis currents. As a consequence, the calculated flux-linkages slightly deviate from the perfect sinusoidal shape as shown in the bottom trace of Fig. 9*b*.

4.3 Power- and torque-speed characteristics

In this section, output power and torque capability of the studied IPMSM under the proposed control method is discussed. Fig. 10 presents power- and torque-speed characteristics of the motor for the speeds above 1000 rpm. The motor delivers a constant torque at the speeds below the base speed of 1500 rpm. A constant power can be obtained from 1500 to 3500 rpm, but above 3500 rpm power starts to drop. Constant power operation is possible until the critical speed of 3500 rpm because maximum current operation can still be possible up to this speed. Beyond this speed, voltage limit ellipses shrink inside the current limit circle, which implies that rated current operation is no longer possible without exceeding the maximum voltage limit of the machine. This is the main reason for the drop of power beyond the critical speed. The speed dependant losses in the machine also increase with speed, which also accounts for reduction in power beyond the critical speed. It was noticed that the maximum operating speed of the motor is 5000 rpm under MTPV control. After 5000 rpm, speed cannot be increased further as the limited torque in the deep flux-weakening region is not sufficient to generate the acceleration required.

5 Conclusion

In this paper, wide-speed operation of a direct torque and flux controlled IPMSM drive was discussed. For a wide speed range,

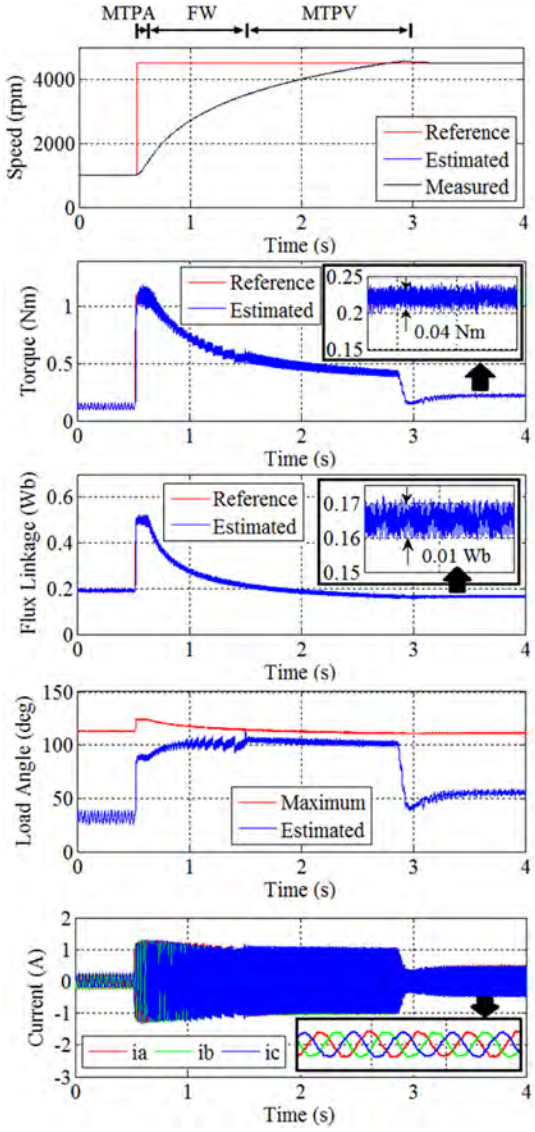

Fig. 7 *Experimental results of acceleration of IPMSM with MTPV control*

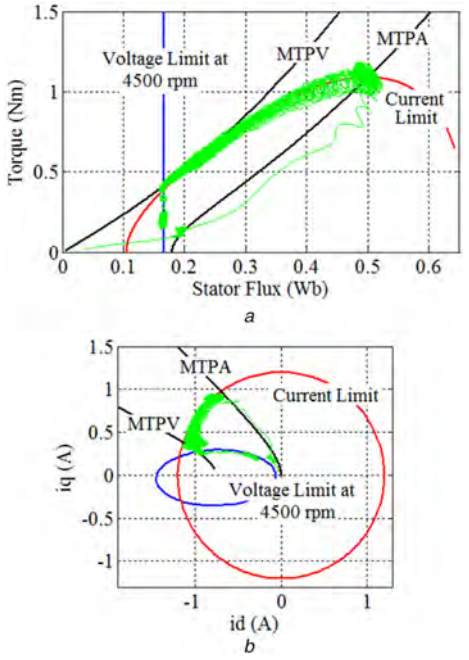

Fig. 8 *Experimental trajectory in*
(a) *T–λ* plane, ***(b)*** i_d–i_q plane for the acceleration of IPMSM from 1000 to 4500 rpm

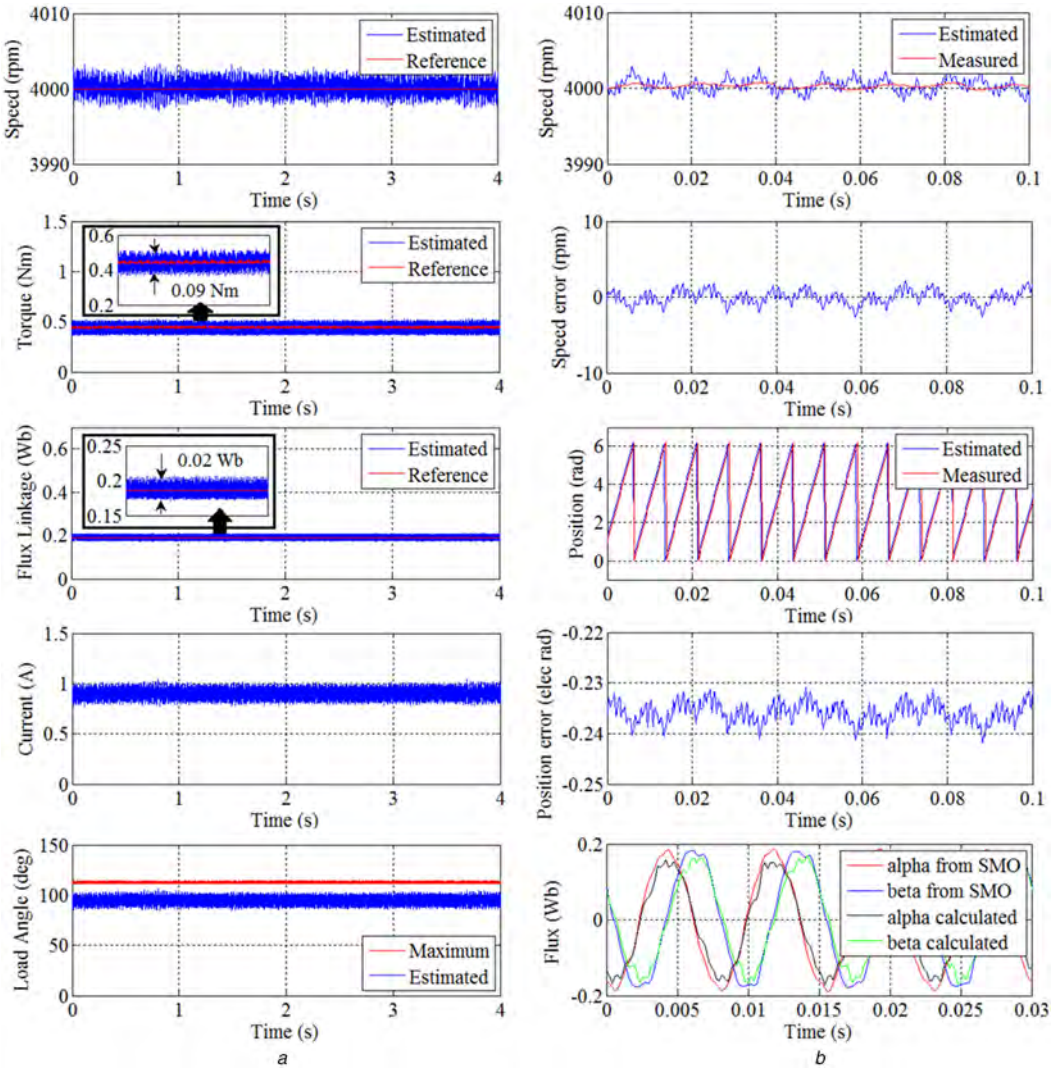

Fig. 9 *Experimental results at 4000 rpm with full load*

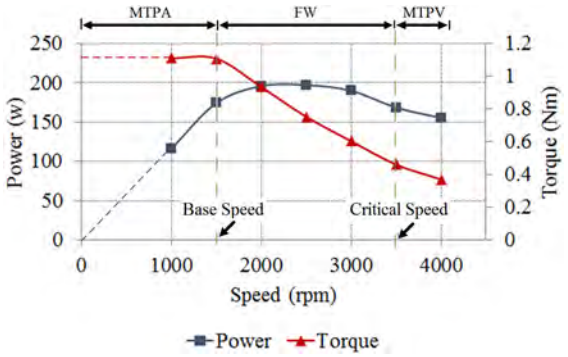

Fig. 10 *Power- and torque-speed characteristics of the IPMSM under sensorless DTFC*

the MTPV trajectory which delivers the optimum performance by minimising flux for maximum torque can be incorporated in the conventional trajectory control of DTFC. It was observed that the load angle of an IPMSM can be indirectly controlled by operating along the trajectories defined on T–λ plane. The operation along MTPV trajectory under DTFC can extend the motor speed to the deep flux-weakening region without violating the maximum load angle condition.

6 References

[1] Inoue, Y., Morimoto, S., Sanada, M.: 'Comparative study of PMSM drive systems based on current control and direct torque control in flux-weakening control region', *IEEE Trans. Ind. Appl.*, 2012, **48**, pp. 2382–2389

[2] Zordan, M., Vas, P., Rashed, M., *et al.*: 'Field-weakening in vector controlled and DTC PMSM drives, a comparative analysis'. Eighth Int. Conf. Power Electronics and Variable Speed Drives, 2000 (IEE Conf. Publ. No. 475), 2000, pp. 493–499

[3] Takahashi, I., Noguchi, T.: 'A new quick-response and high-efficiency control strategy of an induction motor', *IEEE Trans. Ind. Appl.*, 1986, **IA-22**, pp. 820–827

[4] Depenbrock, M.: 'Direct self-control (DSC) of inverter-fed induction machine', *IEEE Trans. Power Electron.*, 1988, **3**, pp. 420–429

[5] Zhong, L., Rahman, M.F., Hu, W.Y., *et al.*: 'Analysis of direct torque control in permanent magnet synchronous motor drives', *IEEE Trans. Power Electron.*, 1997, **12**, pp. 528–536

[6] Lixin, T., Limin, Z., Rahman, M.F., *et al.*: 'A novel direct torque controlled interior permanent magnet synchronous machine drive with low ripple in flux and torque and fixed switching frequency', *IEEE Trans. Power Electron.*, 2004, **19**, pp. 346–354

[7] Buja, G.S., Kazmierkowski, M.P.: 'Direct torque control of PWM inverter-fed AC motors – a survey', *IEEE Trans. Ind. Electron.*, 2004, **51**, pp. 744–757

[8] Das, S.P., Gupta, R.K.: 'Direct torque control (DTC) of interior permanent magnet synchronous motor (IPMSM) with and without speed/position sensors'. 2010 India Int. Conf. Power Electronics (IICPE), 2011, pp. 1–6

[9] Foo, G., Goon, C.S., Rahman, M.F.: 'Analysis and design of the SVM direct torque and flux control scheme for IPM synchronous motors'. Int. Conf. Electrical Machines and Systems, 2009, ICEMS 2009, 2009, pp. 1–6

[10] Jahns, T.M.: 'Flux-weakening regime operation of an interior permanent-magnet synchronous motor drive', *IEEE Trans. Ind. Appl.*, 1987, **IA-23**, pp. 681–689

[11] Morimoto, S., Takeda, Y., Hirasa, T., *et al.*: 'Expansion of operating limits for permanent magnet motor by current vector control considering inverter capacity', *IEEE Trans. Ind. Appl.*, 1990, **26**, pp. 866–871

[12] Jahns, T.M., Kliman, G.B., Neumann, T.W.: 'Interior permanent-magnet synchronous motors for adjustable-speed drives', *IEEE Trans. Ind. Appl.*, 1986, **IA-22**, pp. 738–747

[13] Gallegos-Lopez, G., Gunawan, F.S., Walters, J.E.: 'Optimum torque control of permanent-magnet AC machines in the field-weakened region', *IEEE Trans. Ind. Appl.*, 2005, **41**, pp. 1020–1028

[14] Bing, C., Tesch, T.R.: 'Torque feedforward control technique for permanent-magnet synchronous motors', *IEEE Trans. Ind. Electron.*, 2010, **57**, pp. 969–974
[15] Zhu, L., Xue, S., Wen, X., *et al.*: 'A new deep field-weakening strategy of IPM machines based on single current regulator and voltage angle control'. Energy Conversion Congress and Exposition (ECCE), 2010, 2010, pp. 1144–1149
[16] Dakai, H., Lei, Z., Longya, X.: 'Maximum torque per volt operation and stability improvement of PMSM in deep flux-weakening region'. Energy Conversion Congress and Exposition (ECCE), 2012, 2012, pp. 1233–1237
[17] Ping-Yi, L., Wei-Ting, L., Shang-Wei, C., *et al.*: 'Infinite speed drives control with MTPA and MTPV for interior permanent magnet synchronous motor'. 40th Annual Conf. of the IEEE Industrial Electronics Society, IECON 2014, 2014, pp. 668–674
[18] Rahman, M.F., Zhong, L., Khiang Wee, L.: 'A direct torque-controlled interior permanent magnet synchronous motor drive incorporating field weakening', *IEEE Trans. Ind. Appl.*, 1998, **34**, pp. 1246–1253
[19] Foo, G., Sayeef, S., Rahman, M.F.: 'Wide speed sensorless SVM direct torque controlled interior permanent magnet synchronous motor drive'. 34th Annual Conf. of IEEE Industrial Electronics, 2008, IECON 2008, 2008, pp. 1439–1444
[20] Faiz, J., Mohseni-Zonoozi, S.H.: 'A novel technique for estimation and control of stator flux of a salient-pole PMSM in DTC method based on MTPF', *IEEE Trans. Ind. Electron.*, 2003, **50**, pp. 262–271
[21] Meyer, M., Grote, T., Bocker, J.: 'Direct torque control for interior permanent magnet synchronous motors with respect to optimal efficiency'. European Conf. Power Electronics and Applications, 2007, 2007, pp. 1–9
[22] Zhang, X.N., Foo, G., Douglas, L.M., *et al.*: 'An improved robust field-weakening control algorithm for direct torque controlled IPM synchronous motors'. 2014 Australasian Universities Power Engineering Conf. (AUPEC), 2014, pp. 1–6
[23] Inoue, Y., Ichiya, T., Morimoto, S., *et al.*: 'Wide-speed-range operation of DTC-based PMSM drive system using MTPF control'. 2014 Int. Power Electronics Conf. (IPEC-Hiroshima 2014 – ECCE-ASIA), 2014, pp. 370–375
[24] Ekanayake, S., Dutta, R., Rahman, M.F., *et al.*: 'Operation along the maximum torque per voltage trajectory in a direct torque and flux controlled interior permanent magnet synchronous motor'. 8th IET Int. Conf. Power Electronics, Machines and Drives (PEMD 2016), 2016, pp. 1–6
[25] Quntao, A., Li, S.: 'On-line parameter identification for vector controlled PMSM drives using adaptive algorithm'. 2008 IEEE Vehicle Power and Propulsion Conf., 2008, pp. 1–6
[26] Nguyen, Q.K., Petrich, M., Roth-Stielow, J.: 'Implementation of the MTPA and MTPV control with online parameter identification for a high speed IPMSM used as traction drive'. 2014 Int. Power Electronics Conf. (IPEC-Hiroshima 2014 – ECCE ASIA), 2014, pp. 318–323
[27] Phowanna, P., Boonto, S., Konghirun, M.: 'Online parameter identification method for IPMSM drive with MTPA'. 2015 18th Int. Conf. Electrical Machines and Systems (ICEMS), 2015, pp. 1775–1780
[28] Bolognani, S., Oboe, R., Zigliotto, M.: 'Sensorless full-digital PMSM drive with EKF estimation of speed and rotor position', *IEEE Trans. Ind. Electron.*, 1999, **46**, pp. 184–191
[29] Ilioudis, V.C., Margaris, N.I.: 'PMSM sensorless speed estimation based on sliding mode observers'. 2008 IEEE Power Electronics Specialists Conf., 2008, pp. 2838–2843
[30] Jun, H., Bin, W.: 'New integration algorithms for estimating motor flux over a wide speed range', *IEEE Trans. Power Electron.*, 1998, **13**, pp. 969–977
[31] Xiao, D., Rahman, M.F.: 'Sensorless direct torque and flux control for matrix converter-fed interior permanent magnet synchronous motor using adaptive sliding mode observer'. IEEE PES General Meeting, 2010, pp. 1–5